



Corrosion Inhibition of Pipeline Carbon Steel (N80) in CO₂-Saturated Chloride (0.5 M of KCl) Solution Using Gum Arabic as a Possible Environmentally Friendly Corrosion Inhibitor for Shale Gas Industry

Gaetano Palumbo , Marcin Górný, and Jacek Banaś

(Submitted March 12, 2019; in revised form August 19, 2019; published online October 16, 2019)

The inhibition effect of gum arabic (GA) was investigated using weight loss measurements and electrochemical techniques. The results show that the inhibition efficiency of GA increased with an increase in the concentration of the inhibitor but decreased with the temperature. Immersion time was found to have a profound effect on the corrosion inhibition performance of the inhibitor. Polarization measurements revealed that GA was a mixed-type inhibitor, with higher influence on the anodic reaction. The inhibitor followed the Temkin's adsorption isotherm, and the values of the standard free adsorption energy indicate a mixed-type adsorption, with the physical adsorption being more dominant. SEM-EDS and FT-IR measurements were also employed to support the findings.

Keywords carbon dioxide corrosion, corrosion inhibition, gum arabic

1. Introduction

Conventional natural resource stocks have been on a downward curve to depletion in the past 10 years, especially with huge increases in demand, meaning that alternatives have had to be found. Shale gas has been proposed as one alternative that may be a dependable source in the future and answers the challenge of meeting energy needs. Hydraulic fracturing (HF) technology has been the reason why shale has become a resource with great potential. In the HF process, a pressurized fluid is injected into the wellbore to induce artificial cracks within the reservoir and then the fluid is pumped out allowing the gas to flow out (Ref 1-3). Despite its poor corrosion resistance, carbon steel is broadly used as pipeline material in the shale gas industry infrastructures due mainly to its high

strength, durability, ductility and low cost (Ref 4-8). One of the most common problems found in the exploitation of the shale gas reservoirs is the use of corrosive fluids with high concentrations of chlorides containing carbon dioxide (Ref 9, 10). The fluid usually used in the HF process is mainly a neutral water-based chloride solution (up to 4% of potassium chloride) with different additives (i.e., corrosion inhibitors, thickening agents, inhibitors of scaling, etc. (Ref 5). CO₂ could result from the microbial degradation of hydrocarbon sources present in the environment (Ref 11). The presence of high chloride concentrations in the fluid can lead to a severe corrosion attack to the steel structure, which may be general or localized in nature. Moreover, CO₂ gas dissolves in the fluid to form carbonic acid (H₂CO₃), which further accelerates the corrosion of the steel. This type of corrosion is known as sweet corrosion. The literature reports that the corrosion rate in chlorides containing fluids increases exponentially in the presence of CO₂ (Ref 9). The use of corrosion inhibitors is one of the most cost-effective and practical methods for controlling CO₂ corrosion in the oil and gas industry. The typical commercial inhibitors so far used in the oil/gas field to inhibit CO₂ corrosion occurring in internal carbon steel pipelines are nitrogen-based compounds (Ref 12-16). The literature reports that these inhibitors exhibit excellent anti-corrosion properties (Ref 12-16). However, some of these inhibitors were recognized from the Environment European Commission (EEC) as toxic and potentially dangerous to both the environment and human health. Due to these serious threats, the EEC, with the directive 76/464/EEC, has therefore limited the use of such inhibitors. These concerns have led many researchers to focus their studies toward the development of more environmentally friendly corrosion inhibitors for CO₂ corrosion of the steel. Over the last decade, many natural and low-risk potential corrosion inhibitors have been investigated for carbon steel and steel alloy in different corrosive environments. Naturally occurring polymers such as guar gum (Ref 8, 17-20), Raphia Hookeri (Ref 21), xanthan gum (Ref 22), Plantago (Ref 23), sodium carboxymethyl cellulose (Ref 24)

Electronic supplementary material The online version of this article (<https://doi.org/10.1007/s11665-019-04379-3>) contains supplementary material, which is available to authorized users.

Gaetano Palumbo and **Jacek Banaś**, Department of Chemistry and Corrosion of Metals, Faculty of Foundry Engineering, AGH University of Science and Technology, 30-059 Kraków, Poland; and **Marcin Górný**, Department of Cast Alloys and Composites Engineering, Faculty of Foundry Engineering, AGH University of Science and Technology, 30-059 Kraków, Poland. Contact e-mails: gpalumbo@agh.edu.pl, mgorny@agh.edu.pl, and jbs@agh.edu.pl.

were found to be effective corrosion inhibitors in acid solutions. The results reveal that the corrosion inhibition mechanism was attributed to the strong adsorption of the inhibitor molecules on the active sites of the metal surface, thereby hindering the cathodic and/or anodic reactions on the metal surface (Ref 25-31). It is known that polymers are adsorbed stronger than their monomer analogs. Unlike small molecules, polymers can cover larger surface areas on the metal surface due to their multiple adsorption sites for bonding with the metal surface (Ref 20). Therefore, it is expected that polymers will be better corrosion inhibitors than their monomer analogs (Ref 32). In this regard, researchers seem to have focused their studies more on the use of plant extracts to prevent sweet corrosion (Ref 33-35). Hence, the use of natural polymers to prevent sweet corrosion for the steel in saline media is scanty (Ref 36). Umoren et al. (Ref 36) assessed the inhibition effect of natural polysaccharides as chitosan and carboxymethyl cellulose (CMC) for pipeline steel in CO₂ saturated saline solution. The results from the electrochemical and surface analysis revealed that these inhibitors reduced the corrosion of the steel to some extent by the formation of a protective layer on the metal surface. Gum arabic (GA) is a water-soluble complex mixture of carbohydrates and glycoprotein, with a widespread application in the food, pharmaceutical and cosmetics industries (Ref 25-28). GA is also broadly used in the fracturing fluid as a thickening agent (Ref 2). Over the last years, as witnessed by an increasing number of publications, GA is also emerging as a promising candidate as an environmentally friendly corrosion inhibitor of the metal infrastructures (Ref 25-29, 31). In addition, GA being a biodegradable, non-toxic organic compound provides more environmental benefits than the common toxic inorganic inhibitors, with great benefits for the environment (Ref 37, 38). The studies concerning the use of GA as a corrosion inhibitor have been performed, so far, only in concentrated acidic solutions (Ref 25-28). These studies report that GA proved to be an effective corrosion inhibitor on mild steel and aluminum in both HCl and H₂SO₄ solutions (Ref 24). After an extended literature survey, we concluded that no work on the inhibition capability of GA in chlorides containing carbon dioxide solution for pipeline carbon steel has been reported. Therefore, the purpose of the present paper is to study the effectiveness of GA as a corrosion inhibitor to mitigate sweet corrosion for pipeline carbon steel in a saline solution. This paper aims to show that GA not only can be used as a thickening agent, but it could also be used as an active component in corrosion inhibitor in the shale gas industry. To this end, the study was carried out using weight loss and electrochemical techniques, e.g., electrochemical impedance spectroscopy (EIS) and potentiodynamic polarization (PDP). To assess the maximum possible inhibition efficiency as a function of the concentration of GA, the experiments were performed in uninhibited and inhibited solutions, at the presence of different inhibitor concentrations (i.e., from 0.2 up to 1.0 g L⁻¹). Moreover, the effect of time (i.e., up to 168 h) and temperature on the inhibition efficiency of GA has also been taken into account. This study also aims to explain the mode of the adoption of GA on the metal; thus, the adsorption isotherm and the thermodynamic parameters (i.e., E_a and Q_{ads}) were calculated and discussed. FT-IR analysis was used to gain useful information on the mode of adoption of GA on the metal surface. SEM-EDS measurements were also employed to support the gravimetric and electrochemical results.

2. Experimental Procedures

2.1 Material and Solution

The study was carried out on carbon steel (N80) with composition of (wt.%): C 0.39%, Si 0.26%, Mn 1.80%, Cr 0.04%, V 0.19%, Ni 0.04%, Mo 0.003%, Al 0.03%, Cu 0.26%, Co 0.002%, Sn 0.004%, P 0.001%, S 0.001%, and the remainder Fe. The microstructure of the N80 pipeline steel is composed by cementite (Fe₃C) and ferrite (α -Fe), where the ferritic phase accounts for circa 41% as shown in Fig. 1. The samples used in this study were obtained from pipeline carbon steel (N80) and embedded in a PTFE cylinder block, with the flat surface (0.50 cm²). Each time prior to a test, the exposed surface was ground with silicon carbide abrasive paper up to 1200 grit and then was ultrasonically washed in acetone, rinsed with distilled water and dried. All experiments were carried out in 0.5 M of KCl. The aggressive solution was prepared from reagent grade material potassium chloride (Sigma-Aldrich) and pure deionized water with an electrical resistivity of 0.055 μ S cm⁻¹ at $T = 25$ °C. Gum arabic was purchased from Sigma-Aldrich. The concentrations of the inhibitor solution prepared and used for the study ranged from 0.2 to 1.0 g L⁻¹. Prior to each experiment, CO₂ was purging in the test solution for 1 h and then the purging was maintained throughout the test to minimize the ingress of air. After saturation, the conductivity and pH of the blank solution were 60.30 mS cm⁻¹ and 4.5, respectively. The addition of the inhibitor had a negligible effect on the conductivity and pH.

2.2 Gravimetric Measurement

The gravimetric experiments were carried out suspending the coupons in an unstirred solution (150 mL) with and without of different concentrations of inhibitor (i.e., 0.2 up to 1.0 g L⁻¹) at 25 and 45 °C. The weight loss was determined by retrieving the coupons after 24 h of immersion, by means of an analytical balance with the accuracy of ± 0.1 mg. The effect of time was carried out in the absence and at the concentration where GA exhibits a maximum in the concentration–efficiency curve (i.e., 0.5 g L⁻¹), by retrieving the coupons after 1, 12, 24, 120 and 168 h of immersion. The corrosion product was removed from the metal surface, and the residual corrosion

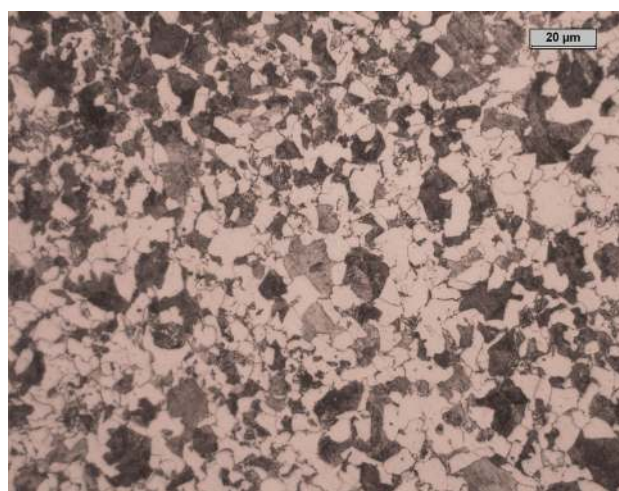


Fig. 1 Microstructure of the N80 pipeline steel sample

product was then removed according to the ASTM G1-90 (Ref 39). The specimen was ultrasonically washed in acetone, rinsed with distilled water, dried and reweighed. In each case, the experiments were conducted thrice and the corrosion rate (CR) was calculated (Ref 26, 28, 29, 31):

$$CR (\text{mg cm}^{-2} \text{h}^{-1}) = \frac{\Delta W}{At} \quad (\text{Eq 1})$$

where ΔW is the weight loss (mg), A is the area of the specimen (cm^2) and t is the exposure time (h). The inhibition efficiency (IE%) was evaluated using the following equation (Ref 26, 28, 29, 31):

$$IE\% = \frac{CR - CR^{\text{inh}}}{CR} \times 100 \quad (\text{Eq 2})$$

where CR^{inh} and CR are the corrosion rates of the steel with and without the inhibitor, respectively.

2.3 Electrochemical Experiments

The electrochemical experiments were performed in a three-electrode cell consisting of a platinum foil as a counter electrode (CE), a saturated calomel electrode (SCE) as a reference electrode and N80 carbon steel used as a working electrode. The measurements were performed on a Gamry reference 600 potentiostat/galvanostat electrochemical system by means of different electrochemical techniques such as impedance spectroscopy (EIS) and potentiodynamic polarization (PDP). The EIS tests were recorded after 24 h of immersion time in the presence and absence of various concentrations of the inhibitor (i.e., 0.2 up to 1.0 g L^{-1}), over the frequency range of 10 kHz to 10 mHz and an amplitude of 10 mV at open circuit potential. To assess the effect of time, the EIS experiments were carried out in the absence and at the optimum GA concentration (i.e., 0.5 g L^{-1}) at a prefixed immersion, i.e., 1, 12, 24, 120 and 168 h and at the same frequency range and amplitude described above. The data were then fitted by means of Echem Analyst 5.21 software using the opportune equivalent circuit. The IE% was calculated from the charge transfer resistance (R_{ct}) determined from the fitting process using the following equation (Ref 25, 30, 31):

$$IE\% = \frac{R_{ct}^{\text{inh}} - R_{ct}}{R_{ct}^{\text{inh}}} \times 100 \quad (\text{Eq 3})$$

where R_{ct}^{inh} and R_{ct} are the charge transfer resistance values in the presence and absence of the inhibitor, respectively. The PDP measurements were performed by sweeping the potential from -1.0 to -0.3 V with a scan rate of 1 mV s^{-1} after holding the specimen at open circuit potential for 24 h (i.e., to assess the effect of GA concentration) and at 168 h (i.e., to assess the effect of time) at open circuit potential. The corrosion current density (j_{corr}), the anodic (β_a) and cathodic (β_c) Tafel constants were determined by means of Echem Analyst 5.21 software. The IE% was calculated from the measured I_{corr} values using the relationship (Ref 25, 30, 31):

$$IE\% = \frac{j_{\text{corr}} - j_{\text{corr}}^{\text{inh}}}{j_{\text{corr}}} \times 100 \quad (\text{Eq 4})$$

where j_{corr} and $j_{\text{corr}}^{\text{inh}}$ represent the corrosion current densities values without and with the inhibitor, respectively.

2.4 Surface Analysis

2.4.1 Fourier Transform Infrared (FT-IR) Spectroscopy. The FT-IR measurements were carried out using Thermo Scientific Nicolet 6700 spectrophotometer equipped with an attenuated total reflectance (ATR) accessory. The FT-IR spectra of the native inhibitor and the adsorbed inhibitor on the metal surface were recorded at a resolution of 4 cm^{-1} , with 128 co-added scans over the range from 3700 to 700 cm^{-1} .

2.4.2 Scanning Electron Microscopy and Energy-Dispersive Spectroscopy (SEM-EDS). The steel specimens, prepared as described above, were investigated after being exposed for 24 and 168 h in the absence and presence of the optimum concentration of the inhibitor (i.e., 0.5 g L^{-1}). After the immersion time had elapsed, the specimens were removed and rinsed with deionized water. The investigation was carried out by using a JEOL scanning electron microscope with the magnification of $2000 \times$, while the chemical compositions of the corrosion product layer were analyzed by an energy-dispersive spectroscopy.

3. Results and Discussion

3.1 Gravimetric Measurement

The corrosion rate and inhibition efficiency for carbon steel (N80) pipeline calculated after 24 h of immersion time in CO_2 -saturated chloride (0.5 M of KCl) solution (blank solution) and with the addition of different concentrations of GA (i.e., from 0.2 up to 1.0 g L^{-1}) are presented in Table 1. It follows from the data that the corrosion rate decreases and the inhibition efficiency increases with an increase in GA concentration, with the maximum inhibitor efficiency found to be 68.78% at 0.5 g L^{-1} of GA. The results are in line with the findings reported in the literature by other researchers. Umoren et al. (Ref 26, 28), in the study concerning the inhibition effect of GA for mild steel in $0.1 \text{ M H}_2\text{SO}_4$ solution, in the weight loss section, reported that the addition of GA, to the free acid solution, reduced the dissolution of the metal and that the extent of its protection varied with the inhibitor concentration. The authors justified the findings based on the presence of heteroatoms such as oxygen and nitrogen in the GA structure that work as adsorptive centers. The authors reported that the inhibition of the steel was ascribed to the adsorption of GA

Table 1 Corrosion rate and inhibition efficiency obtained from weight loss measurements for carbon steel (N80) at various concentrations of GA after 24 h of immersion time at 25-45 °C

| $C_{\text{inh}}, \text{g L}^{-1}$ | Corrosion rate, $\text{mg cm}^{-2} \text{h}^{-1}$ | | IE, % | |
|-----------------------------------|---|-------|-------|-------|
| | 25 °C | 45 °C | 25 °C | 45 °C |
| Blank | 0.378 | 0.434 | ... | ... |
| 0.2 | 0.217 | 0.384 | 42.59 | 20.37 |
| 0.3 | 0.172 | 0.343 | 54.50 | 29.63 |
| 0.4 | 0.147 | 0.323 | 61.11 | 37.04 |
| 0.5 | 0.118 | 0.333 | 68.78 | 40.74 |
| 0.9 | 0.128 | 0.343 | 66.14 | 38.89 |
| 1.0 | 0.118 | 0.434 | 68.78 | 37.04 |

molecules through these adsorptive centers. In this study, the increase in the IE% with increasing the concentration of GA can be ascribed to a gradual increase in the surface coverage due to its adsorption on the metal surface thus reducing the contact between the aggressive solution and the metal surface. It is worth mentioning that the authors, at the same experimental conditions (i.e., after 24 h of immersion and at the same temperature), reported a maximum inhibition efficiency of 21.9% at 0.5 g L⁻¹ of GA, which is circa three times lower than that reported in this study. The higher value of the IE% shown by GA in this study can be attributed to the different nature of the anions involved in the adsorption process. Electronegative ions may adsorb on the positive metal surface changing the surface of the metal from positive to negative. These negative charges will favor the adsorption of the protonated inhibitor. Chloride ions have a smaller degree of hydration; therefore, the number of chloride ions adsorbed on the metal surface is thought to be higher than that of the sulfate ions (Ref 40, 41). Gum inhibitors are reported to be adsorbed on the metal surface mainly via electrostatic interaction established between the adsorbed anions and the inhibitor molecules (Ref 21, 25, 26, 29, 42). Therefore, the higher value of the IE% observed in this study may be due to the fact that the number of protonated inhibitor molecules adsorbed on the metal surface will be higher in the chlorides-containing solution than that of the sulfate solution. Moreover, Table 1 also reveals that the value of the IE% decreases upon increasing the temperature of the tested solution, with the maximum value found to be 38.0% at 0.5 g L⁻¹ of GA. It has been reported (Ref 22, 23, 26) that the inhibitor molecules are continuously adsorbed and desorbed on the metal surface and that this equilibrium is temperature dependent. It seems that for GA, upon increasing the temperature, the desorption of the inhibitor molecules is more favored than that of their adsorption, leading to a less stable adsorbed layer. According to the literature, the decrease in the IE% at a higher temperature is an indication of a physical adsorption mechanism (Ref 22, 23, 26).

3.2 Adsorption Study and Standard Adsorption Free Energy

In the present study, the nature of the adsorption of GA on the corroding N80 carbon steel surface in the tested solution was assessed by several adsorption isotherms, namely Langmuir, Frumkin, Temkin, Flory–Huggins, Freundlich and El-Awady adsorption isotherm (Ref 25, 27). Of all the adsorption isotherms tested, the Temkin's adsorption isotherm was found to give the best description of the adsorption behavior of the studied inhibitor. The Temkin's adsorption isotherm is defined by the following equations:

$$\theta = \frac{-2.303 \log K_{\text{ads}}}{2a} - \frac{2.303 \log C}{2a} \quad (\text{Eq 5})$$

where θ is the surface coverage degree ($\theta = \text{IE\%/100}$), C is the inhibitor concentration, K_{ads} the adsorption–desorption equilibrium constant, a is the molecules interaction parameter. Positive values of a imply attractive forces between the inhibitor molecules, while negative values indicate repulsive forces between them. The thermodynamic parameters obtained from the Temkin's isotherm for the studied inhibitor, calculated from the weight loss at different temperatures, are given in Table 2 and displayed in Fig. 2. The regression coefficient ranges between 0.995 and 0.994 at 25 and 45 °C, respectively. It follows from the table that the values of a are negative in both

Table 2 Temkin's adsorption isotherm parameters calculated from weight loss measurements after 24 h of immersion time

| Temperature, °C | a | K_{ads} , L g ⁻¹ | ΔG_{ads} , kJ mol ⁻¹ |
|-----------------|--------|--------------------------------------|--|
| 25 | - 1.79 | 23.00 | - 24.90 |
| 45 | - 2.21 | 12.36 | - 23.36 |

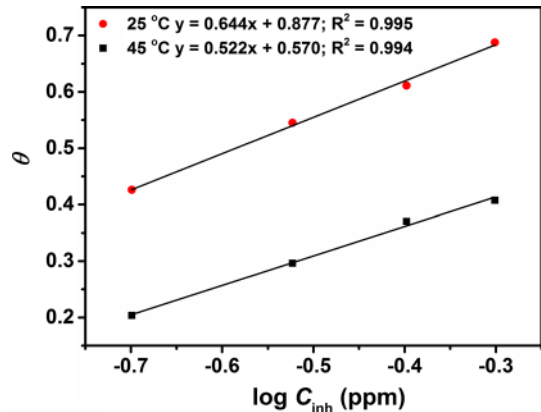


Fig. 2 Adsorption Temkin's isotherm carbon steel (N80) pipeline steel in CO₂-saturated chloride (0.5 M KCl) at 25–45 °C

temperatures, which is an indication of the repulsive forces between the adsorbed molecules.

The equilibrium constant, K_{ads} , for the adsorption process of the inhibitor is related to the free energy of adsorption (ΔG_{ads}) with the following relationship:

$$\Delta G_{\text{ads}}^{\circ} = -RT \ln(1 \times 10^3 K_{\text{ads}}) \quad (\text{Eq 6})$$

where R is the gas constant (8.314 J K⁻¹ mol), T is the absolute temperature (K) and the value 1×10^3 is the concentration of water molecules in the solution expressed in g L⁻¹. It should be noted that for values of $\Delta G_{\text{ads}}^{\circ}$ higher than -20 kJ mol⁻¹, the adsorption process is regarded as a physisorption process while lower than -40 kJ mol⁻¹ indicates a chemisorption process (Ref 25, 26). In the present study, the values of $\Delta G_{\text{ads}}^{\circ}$ presented in Table 2 are -24.90 and -23.36 kJ mol⁻¹ at 25 and 45 °C, respectively. The negative values of $\Delta G_{\text{ads}}^{\circ}$ indicate that the adsorption of GA on the carbon steel surface in the tested solution is a spontaneous process (Ref 25, 26). Moreover, the results indicate that the adsorption mechanism is a mixed-type adsorption (i.e., physical and chemical adsorption), with the physical adsorption being more dominant. The findings observed in this study corroborate the earlier reports found in the literature (Ref 18, 19, 25, 26).

3.3 Activation Parameters

The values of the activation energy were calculated with the help of the linearized Arrhenius equation:

$$\log \frac{\text{CR}_2}{\text{CR}_1} = \frac{E_a}{2.303R} \left(\frac{1}{T_1} - \frac{1}{T_2} \right) \quad (\text{Eq 7})$$

where CR_1 and CR_2 are the values of the corrosion rates at temperature T_1 (25 °C) and T_2 (45 °C), respectively. E_a is the

apparent activation energy, R is the gas constant ($8.314 \text{ J mol}^{-1} \text{ K}^{-1}$).

The values of the heat of adsorption were calculated using the following equation

$$Q_{\text{ads}} = 2,303R \left[\log \left(\frac{\theta_2}{1-\theta_2} \right) - \log \left(\frac{\theta_1}{1-\theta_1} \right) \right] \times \left(\frac{T_1 \times T_2}{T_2 - T_1} \right) \quad (\text{Eq 8})$$

where θ_1 and θ_2 are the values of the surface coverage degree at temperatures T_1 ($25 \text{ }^\circ\text{C}$) and T_2 ($45 \text{ }^\circ\text{C}$), respectively. Table 3 lists the values of E_a and of Q_{ads} . It follows from the data that: (1) the values of E_a are higher in the presence of GA than for the blank solution; (2) E_a increases with increasing the concentration of the inhibitor; (3) the values of Q_{ads} are negative for all the studied range of GA concentration.

It has been reported that the increase in E_a after the addition of the inhibitor indicates either a physical adsorption process or the formation of weak chemical bondings between the inhibitor molecules and the metal surface (Ref 24). These results, combined with the trend of the decreased in inhibition efficiency with an increase in temperature and the negative values of Q_{ads} , further support the proposed physical adsorption nature of the process (Ref 22, 24).

3.4 EIS Measurement

Figure 3 shows the EIS measurements carried out on carbon steel (N80) in CO_2 -saturated chloride (0.5 M of KCl) solution with different concentrations of GA. Figure 3(a) reveals that the shape of the Nyquist plots does not change after the addition of GA into the tested solution, suggesting that its addition does not

Table 3 Thermodynamic parameters for carbon steel (N80) pipeline steel in CO_2 -saturated chloride (0.5 M KCl) solution in the absence and presence of GA from weight loss measurements

| C_{inh} , g L^{-1} | E_a , kJ mol^{-1} | ΔQ_{ads} , kJ mol^{-1} |
|--------------------------------------|------------------------------|--|
| Blank | 5.45 | ... |
| 0.2 | 22.51 | - 41.99 |
| 0.3 | 27.22 | - 41.23 |
| 0.4 | 31.05 | - 38.75 |
| 0.5 | 40.92 | - 45.93 |
| 0.9 | 38.87 | - 44.23 |
| 1.0 | 51.36 | - 52.07 |

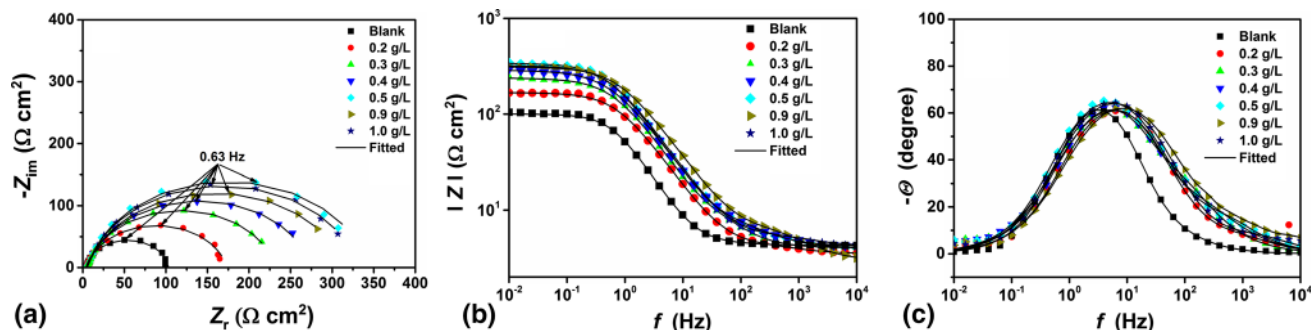


Fig. 3 Impedance plots recorded at OCP after 24 h of immersion for carbon steel (N80) pipeline steel in CO_2 -saturated chloride (0.5 M KCl) solution in the absence and presence of various concentrations of GA. (a) Nyquist, (b) Bode and (c) phase angle representations at $25 \text{ }^\circ\text{C}$

alter other aspects of the corrosion mechanism. The EIS parameters calculated from the analysis of the impedance spectra fitted with the help of the equivalent circuit shown in Fig. 4 are listed in Table 4. Due to the imperfection of the metal surface, the double layer capacitance (C_{dl}) is simulated using a constant phase element (CPE) (Ref 18, 24). The impedance of CPE is described by the following equation:

$$Z_{\text{CPE}} = \frac{1}{Q(j\omega)^n} \quad (\text{Eq 9})$$

where Q stands for CPE constant, n is the exponent, j is the imaginary number, and ω is the angular frequency at which Z reaches its maximum value. The parameter n quantifies the imperfections of the surface. For $n = 1$, CPE is a pure capacitor, and for $n = -1$, CPE is an inductor. The values of the double layer capacity were calculated from the following equations (Ref 25):

$$C_{\text{dl}} = Q(2\pi f_{\text{max}})^{n-1} \quad (\text{Eq 10})$$

where f_{max} represents the frequency at which Z reaches its maximum value on the Nyquist plot. As shown from Fig. 3, the fitted results present similar shape with those obtained experimentally with the values of the “goodness of fit” chi-squared (χ^2) found to be very low (Table 4). This clearly indicates that the equivalent circuit used to simulate the system under investigation is the most appropriate one. From the plots, it is clear that the impedance of the steel in the blank solution changes significantly after the addition of 0.2 g L^{-1} of GA to the corrosive solution, reflecting an increase in R_{ct} values from 98.91 to $168.70 \text{ } \Omega \text{ cm}^2$ for the blank and inhibited solution,

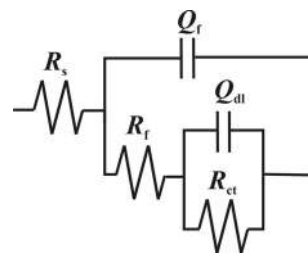


Fig. 4 Equivalent circuit used to fit the EIS plots. Here, R_s is the electrolyte resistance, Q_{dl} is the constant phase element representing the double charge layer capacitance, R_{ct} is the charge transfer resistance, R_f is the layer resistance and Q_f is the constant phase element of the layer

Table 4 Electrochemical parameters and corrosion inhibition efficiency in the absence and presence of different concentrations of GA after 24 h of immersion time

| $C_{inh}, g L^{-1}$ | $R_s, \Omega cm^2$ | $Q_f, m\Omega^{-1} s^n cm^{-2}$ | n_1 | $R_f, \Omega cm^2$ | $Q_{dl}, \mu\Omega^{-1} s^n cm^{-2}$ | n_2 | $R_{ct}, \Omega cm^2$ | $C_{dl}, mF cm^{-2}$ | $\chi^2, 10^{-4}$ | IE, % |
|---------------------|--------------------|---------------------------------|-------|--------------------|--------------------------------------|-------|-----------------------|----------------------|-------------------|-------|
| Blank | 4.26 | 1.10 | 0.94 | 0.44 | 1.85 | 0.93 | 98.91 | 1.68 | 2.8 | ... |
| 0.2 | 3.51 | 0.59 | 0.85 | 1.44 | 1.04 | 0.87 | 168.70 | 0.87 | 4.4 | 41.37 |
| 0.3 | 4.37 | 0.93 | 0.85 | 1.37 | 0.56 | 0.88 | 211.90 | 0.47 | 1.1 | 53.32 |
| 0.4 | 4.20 | 0.68 | 0.82 | 6.44 | 0.53 | 0.89 | 268.40 | 0.50 | 7.0 | 63.15 |
| 0.5 | 4.06 | 0.35 | 0.88 | 4.05 | 0.74 | 0.88 | 332.70 | 0.70 | 1.3 | 70.27 |
| 0.9 | 2.90 | 0.38 | 0.80 | 5.72 | 0.46 | 0.88 | 313.10 | 0.39 | 1.3 | 68.41 |
| 1.0 | 4.30 | 0.22 | 0.80 | 1.75 | 0.82 | 0.86 | 327.30 | 0.68 | 8.9 | 69.78 |

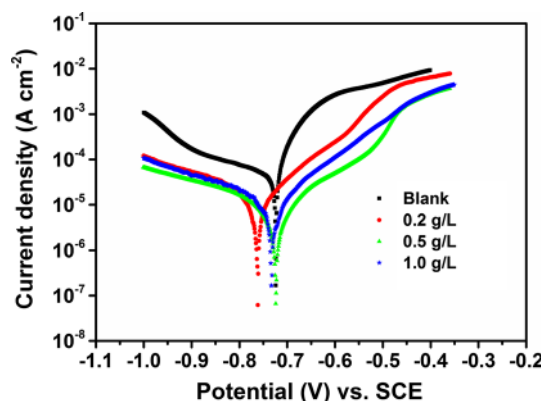


Fig. 5 Potentiodynamic polarization parameters in the absence and presence of different concentrations of GA after 24 h of immersion time

respectively. Moreover, it can be seen that the impedance of the metal increases with an increase in GA concentration. This behavior is likely due to the continuous adsorption of the inhibitor and the continuous growth of a protective layer on the metal surface (Ref 24-29, 31), as also confirmed by the SEM-EDS analyses (Fig. 9c). Inspection of Table 4 also reveals that R_{ct} and C_{dl} have an opposite trend in the whole concentration range. The value of R_{ct} increases while the value of C_{dl} decreases upon increasing the concentration of the inhibitor. The greatest effect was observed at $0.5 g L^{-1}$ of GA. A decrease in C_{dl} , compared to the blank solution, could be due to either an increase in the thickness of the electrical double layer and/or a decrease in the local dielectric constant, according to the Helmholtz model ($C_{dl} = \epsilon\epsilon_0 A/\delta$) (Ref 43). Where ϵ is the dielectric constant of the medium, ϵ_0 the vacuum permittivity, A is the electrode area, and δ is the thickness of the protective layer. This behavior is often ascribed to the replacement of water molecules on the metal/solution interface due to the adsorption of GA molecules on the metal surface (Ref 29, 40, 44). The Bode modulus plots (Fig. 3b) agree with the Nyquist spectra in which it can be seen that the impedance modulus was observed to increase with an increase in GA concentration for the entire frequency range, which indicates that GA reduced the corrosion rate in the inhibited solution. Moreover, the effect of the inhibitor can also be seen from the Bode phase angle plots shown in Fig. 3(c), where the phase angle becomes broader after the addition of the inhibitor. The broadening is likely due to the formation of a porous inhibitor film on the electrode surface.

The inhibition efficiencies calculated from Eq 2 are listed in Table 4. It follows from the data that the IE% gradually increases with an increase in GA concentration up to $0.5 g L^{-1}$, with the maximum value found to be 70.27%. This behavior suggests that the adsorption of GA retards the dissolution of the metal due to the formation of a protective layer on its surface. Moreover, up to $0.5 g L^{-1}$ of GA, the protective layer is strengthened by the further addition of GA, after which it remains almost constant.

3.5 PDP Measurement

The potentiodynamic polarization curves for carbon steel (N80) pipeline in CO_2 -saturated chloride ($0.5 M$ of KCl) solution in the absence and presence of GA are displayed in Fig. 5. The corrosion kinetic parameters calculated from the polarization plots are given in Table 5. The data clearly shows that the addition of GA prominently reduces the values of j_{corr} with the maximum inhibition efficiency of 67.04% achieved at $0.5 g L^{-1}$ of GA. Beyond this critical value, the performance of the inhibitor remains constant for a further increase in GA. Moreover, Fig. 5 also shows that the addition of GA shifts both the cathodic and anodic branches of the polarization curves toward lower current densities compared to the blank solution. It is apparent from the figure that the cathodic current density is markedly reduced even at lower inhibitor concentrations, and it does not change much for further addition of GA. This behavior indicates that the addition of GA does not change the mechanism of the corrosion process and that the hydrogen evolution reaction is in activation-controlled (Ref 25, 45). This suggests that GA forms an adsorptive layer on the metal surface that hinders the hydrogen evolution reaction (Ref 25, 45), as discussed in more detail in section 3.8.2. In contrast, the shape of the anodic curves changed greatly after the addition of GA, suggesting that the dissolution reaction is predominantly retarded. The observations indicate that the addition of the inhibitor hinders both partial reactions (i.e., hydrogen evolution and anodic dissolution) by either covering part of the metal surface and/or blocking the active corrosion sites on the steel surface. Moreover, a closer inspection of the polarization plots shows that in the presence of the inhibitor, a clear inflection is quite visible in the anodic branches (i.e., for potential around -600 to -500 mV). Other authors also reported a similar behavior (Ref 45-47). They defined this potential as the desorption potential. The authors also suggested that, for potentials lower than this desorption potential, the inhibitor hinders the anodic reaction while, beyond this critical potential, the dissolution of the metal occurs. The dissolution may be attributed to the desorption of the adsorbed inhibitor layer from

Table 5 Potentiodynamic polarization parameters in the absence and presence of different concentrations of GA after 24 h of immersion time

| C_{inh} , g L ⁻¹ | β_c , mV dec ⁻¹ | β_a , mV dec ⁻¹ | I_{corr} , $\mu\text{A cm}^{-2}$ | E_{corr} , mV SCE ⁻¹ | IE, % |
|-------------------------------|----------------------------------|----------------------------------|------------------------------------|-----------------------------------|-------|
| Blank | 0.318 | ... | 37.90 | - 724 | ... |
| 0.2 | 0.334 | 0.128 | 17.11 | - 761 | 54.85 |
| 0.5 | 0.326 | 0.164 | 12.49 | - 724 | 67.04 |
| 1.0 | 0.291 | 0.131 | 12.55 | - 732 | 66.89 |

the metal surface (Ref 45-47). It should be noted that in the case of the uninhibited solution, the anodic polarization curve does not show the typical Tafel behavior; therefore, the corrosion current density was calculated from the extrapolation of the cathodic Tafel region according to Amin et al. (Ref 45). Table 5 shows that the E_{corr} shifts toward both the cathodic and anodic regions with no definite trend after the addition of various concentrations of the inhibitor, indicating that GA is a mixed-type inhibitor (Ref 25, 31). The literature reports (Ref 18, 25) that, if the shift of the E_{corr} in the presence of the inhibitor was bigger than ± 85 mV, compared to the E_{corr} of the blank solution, the inhibitor is regarded either as a cathodic or an anodic type. In this study, the shift is less than 85 mV, which further support the mixed-type nature of the tested inhibitor.

3.6 Effect of Time

Immersion time plays an important role in assessing the stability of the inhibitive behavior of a given corrosion inhibitor. The effect of immersion time on the corrosion inhibition of N80 carbon steel in a CO₂-saturated chloride (0.5 M of KCl) solution by gum arabic was determined using both gravimetric and electrochemical techniques at a prefixed immersion time (e.g., 1, 12, 24, 120, 168 h). The experiments were carried out at 0.5 g L⁻¹ of GA, which is the concentration in which GA exhibits a maximum in the concentration–efficiency curve.

3.6.1 Gravimetric Measurement. Table S1 (supplementary information) shows the corrosion rate and the inhibition efficiency as a function of immersion time in the absence and presence of the inhibitor. It is apparent from the table that CR in the absence of the inhibitor increases with an increase in immersion time. Form Fig. 1, it can be seen that the N80 carbon steel has a ferrite–pearlite microstructure, with 41% of the ferritic phase. The ferritic phase is known to be more active than the iron carbide contained in the eutectoid mixture (Ref 10). The increase in the corrosion rate with time has been attributed to a micro-galvanic effect established between these two phases, with the ferrite phase acting as an anode and the cementite as a cathode (Ref 10, 48). Over time, the uncontrolled selective dissolution of the ferrite phase leads to an increase in Fe₃C over the metal surface, which will eventually create a vicious circle (Ref 48-54). The growth of the cementite layer on the metal surface causes an increase in the cathodic area, which in turn, accelerates the dissolution of the steel and so on. (Ref 10, 48). By contrast, it follows from the data shown in Table S1 that upon the introduction of GA into the system, the corrosion rate of the metal decreases, which indicates that GA is an effective corrosion inhibitor, isolating the metal surface from the attack of the aggressive solution. Inspection of Table S1 also reveals that, at the optimum concentration, the

inhibition efficiency increases with an increase in immersion time and attains an optimum value at 120 h (90.76%) after which, for further increase in immersion time, no appreciable change is observed. The results clearly indicate that a continuous formation of an inhibitor protective layer on the metal surface occurs during the first 120 h, after which the active sites on the surface are almost occupied by the inhibitor and therefore the corrosion process becomes stable. Table S3 (supplementary information) lists the inhibition efficiency and the time of exposure at which the maximum inhibition efficiency has been calculated of various corrosion inhibitors derived from natural products. It follows from the table that these studies were mostly performed at short immersion times (i.e., up to 6 h) and only a few of them were carried out at long immersion (i.e., 168 h). It can be seen from the table that, compared to other natural corrosion inhibitors, GA can be considered a good environmentally friendly corrosion inhibitor for carbon steel in a CO₂-saturated chloride solution over prolonged exposure times.

3.6.2 EIS Measurement. Figure 6 presents the impedance responses observed at 1, 12, 24, 120 and 168 h of immersion in the absence and presence of 0.5 g L⁻¹ of GA. Table S2 (supplementary information) lists parameters calculated from the analysis of the impedance plots with the use of the equivalent circuit presented in Fig. 4. It can be seen from Fig. 6(a) that the mechanism of the corrosion process in the presence of GA did not change with the immersion time, since the shape of the Nyquist plots, in its presence and absence, remains unchanged. Nyquist plots also show that immersion time plays a significant role in the corrosion resistance of the steel in the case of the investigated concentration. For instance, it follows from Table S2 that in the presence of 0.5 g L⁻¹ of GA, R_{ct} gradually increases with an increase in immersion time, going from 144.60 $\Omega\text{ cm}^2$ (1 h) up to 417.10 $\Omega\text{ cm}^2$ after 120 h of immersion, reflecting an increase in inhibition efficiency from 57.90 to 90.60%. After 120 h, the value of R_{ct} reaches a certain value and it does not change much over time. The increase in the IE% with increasing of immersion time suggests that GA molecules are progressively adsorbed on the metal surface, leading to the formation of a thicker protective layer after 168 h of immersion, compared to the uninhibited solution (Ref 18, 24, 44). In contrast, in the absence of the inhibitor, the values of R_{ct} gradually decrease with the immersion time. This behavior can be ascribed to the formation of a less thick and/or stable protective layer on the metal surface as confirmed from the cross section analysis (Fig. 10c and d) (Ref 25, 26, 49). The Bode phase angle plot shown in Fig. 6(c) reveals that in the case of the uninhibited solution, the size of the phase angle does not change much over time, with a phase angle maxima close to 46° after 168 h of immersion. Con-

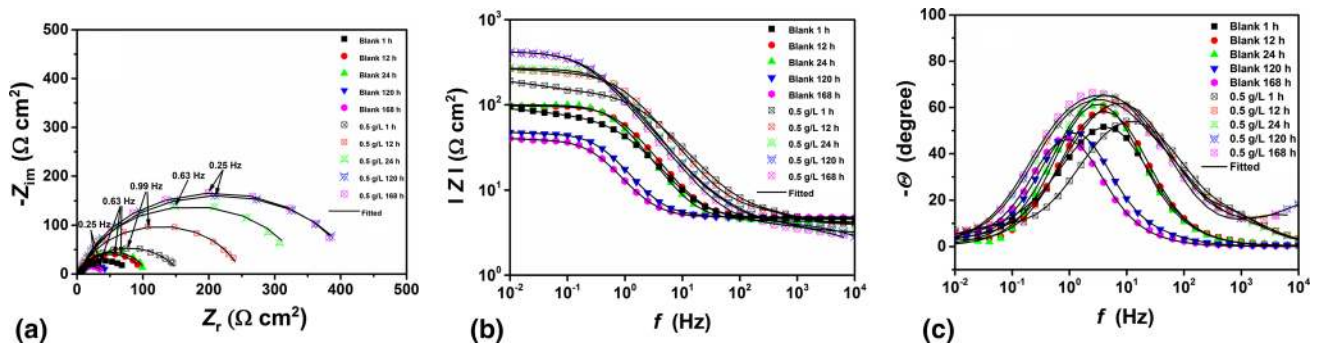


Fig. 6 Impedance plots recorded for carbon steel (N80) pipeline steel in CO₂-saturated chloride (0.5 M KCl) solution in the absence and presence of 0.5 g L⁻¹ of GA as function of time. (a) Nyquist, (b) Bode and (c) phase angle representations at 25 °C

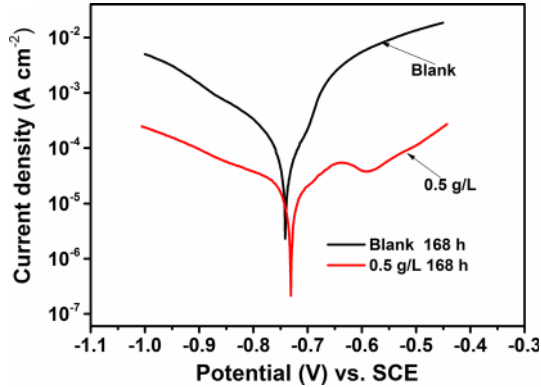


Fig. 7 Polarization curves for carbon steel (N80) pipeline steel in CO₂-saturated chloride (0.5 M KCl) solution in the absence and presence of 0.5 of GA as function of time (up to 168 h)

versely, the size of the phase angle becomes broader and bigger with time for the inhibited solution, with a phase angle maxima close to 70° after 168 h of immersion. It should be noted that in the case of an ideal capacitor, the phase angle maxima in the intermediate frequencies is 90° (Ref 36, 55). The inhibitor system under study showed a wider capacitive behavior, compared to the blank solution, suggesting an improvement in the capacitive performance in the presence of the inhibitor with time. Therefore, the approach of the phase angle values toward 90° in the presence of GA reflects a strong molecular adsorption and thus the formation of a thicker and/or a more compact protective layer on the steel/electrolyte interface after long exposure times.

It is worth mentioning that Bentrach et al. (Ref 25) observed, after 1 h of exposure, a maximum inhibition efficiency of 91% at 1.5 g L⁻¹ of GA. Beyond this critical value, the IE% was constant. Moreover, at 0.5 g L⁻¹ of GA Bentrach reported an inhibition efficiency of 79%, after 1 h of immersion, against an inhibition efficiency of 57.72% reported in this study, at the same concentration of GA and exposure times. The higher value of the IE% observed by Bentrach and co-authors can be ascribed to the higher concentration of chloride ions and lower pH (i.e., a higher concentration of H⁺ ions in the solution). As mentioned before, Gum inhibitors are mainly adsorbed on the metal surface via electrostatic interaction between the charged metal surface and the charged inhibitor molecules. Therefore, an increase in concentration of both Cl⁻ and H⁺ ions increases the number of inhibitor molecules adsorbed, hence the

inhibition efficiency. A similar result was also reported by Abu-Dalo et al. (Ref 31).

3.6.3 PDP Measurement. Figure 7 shows the corrosion potentiodynamic measurement without and with the addition of 0.5 of GA after 168 h of immersion. The potentiodynamic parameters calculated from the curves are given in Table S4 (supplementary information). The data show that the corrosion current density decreases in the presence of GA, compared to the blank solution. Moreover, both the cathodic and anodic curves shift to lower corrosion current densities. This behavior indicates that after 168 h of immersion, GA still has a significant effect on both partial reactions of the corrosion process. Thus, GA reduced the mechanism of the hydrogen evolution and the anodic dissolution of the steel (Ref 10, 56). In addition, Fig. 7 shows that the shape of the cathodic portion does not change with the addition of GA. However, the shape of the anodic domain changed greatly in the presence of 0.5 g L⁻¹ of GA compared to the blank solution. At the optimum concentration of GA, and over a long immersion time, the metal exhibits a pseudo-passive region, only, extends to a small range of potential (i.e., -650 to -550 mV). This change in the shape of the anodic branch can be explained by the fact that after 168 h of immersion, a thicker adsorptive layer is formed on the metal surface (Ref 25, 26, 49), as also confirmed by the cross section analyses presented in Fig. 10(d). An increase in thickness could prevent the diffusion of the aggressive species from the bulk solution to the metal surface and therefore, limiting the dissolution of the metal. However, at a potential higher than circa -550 mV (e.g., the desorption potential), the current increases again with the potential, which means that the dissolution of the metal occurs likely due to the desorption of the adsorbed inhibitor layer from the surface. On the other hand, the absence of this pseudo-passive region in the absence of GA points to the formation of a less thick and stable adsorbed layer (Ref 25, 26, 49) (Fig. 10c).

3.7 Surface Analysis

3.7.1 FT-IR Measurement. The FT-IR spectra of the pure GA and the adsorbed GA on the metal surface are shown in Fig. 8. Differences between the two spectra can be used to gain useful information regarding the adsorption mechanism of GA to the metal surface. The spectrum of the native GA shows a peak at 3302 cm⁻¹ ascribed to the extensive intramolecular hydrogen bonds and stretching vibration of the -OH groups (Ref 17, 20). The peak at 2919 cm⁻¹ is attributable to the vibration mode of the C-H bonds. The peaks at 1597 cm⁻¹ and

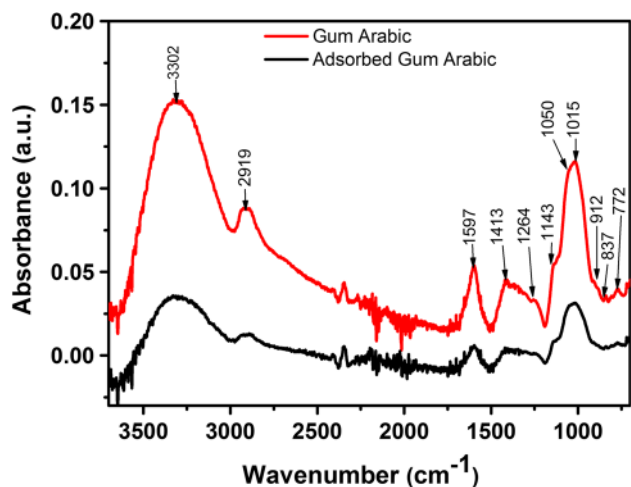


Fig. 8 FT-IR spectra of native gum arabic and surface-adsorbed gum arabic

at 1413 cm^{-1} are attributable to the asymmetric and symmetric stretching vibration of the carboxylic groups (COOH) of GA (Ref 57, 58). From the spectrum of the native inhibitor, a broad peak between 1400 and 1200 cm^{-1} can be seen likely due to the band assigned to the O–H in-plane bending vibration and the band of –CH₂– scissoring vibration that overlaps each other (Ref 17). The bands at 1143 , 1050 , 1015 cm^{-1} are due to the symmetrical and asymmetrical ring breathing vibrations of C–C–O and C–O–C (Ref 57). The (Ref 20) bands at 1050 and 1015 cm^{-1} are due to the stretching vibration of C–O (Ref 57). The peaks at 912 , 837 , 772 cm^{-1} can be associated with the glucoside (1-4) linkage of the galactose unit and the (1-6) linkage of the mannose unit (Ref 18, 59). The characteristic bands related to the primary (3400 – 3500 cm^{-1}) and secondary (3310 – 3350 cm^{-1}) amine groups of the protein fraction (i.e., glycoprotein) are not visible due to swamped of these peaks by the adsorption of the O–H groups of the saccharide units (Ref 31, 60). Figure 8 shows that the spectrum of the adsorbed GA presents all the characteristic peaks shown by the native GA although with a lower intensity. Some authors (Ref 17, 20, 31) reported that the decrease in intensity of the peak observed at 3302 cm^{-1} may be due to the binding of some of the hydroxyl groups of GA with the metal surface via the H bonds formation (Ref 17, 18, 20). The decrease in intensity of the characteristic peaks of gum arabic at 1597 and 1413 cm^{-1} may also be attributed to the formation of hydrogen bonds between the carboxylic groups of GA and the oxidized metal surface, as also reported by other researchers (Ref 31, 45, 61). Some authors have attributed the decrease in intensity of the peaks between 1143 and 772 cm^{-1} to a possible interaction between the endocyclic oxygen atom of the galactose unit of GA and C6–O of the monosaccharide unit with the surface (Ref 17, 18). The results are in agreement with the previous works regarding the adsorption of gum inhibitors on the steel surface (Ref 17, 18, 20, 31).

3.7.2 SEM–EDS Morphology. SEM–EDS measurements were also employed in order to support the electrochemical and gravimetric measurements reported in this study. A SEM image of the freshly polished surface of the steel is shown in Fig. 9(a). The image clearly shows the presence of parallel scratches on the steel surface due to the polishing

process; however, no noticeable defects can be seen on the metal surface. Figure 9 also shows the surface morphological examinations of the steel surface in the absence (b) and presence (c) of 0.5 g L^{-1} of GA after 24 h of immersion at $25\text{ }^{\circ}\text{C}$. The microstructure of the sample is partially revealed after the corrosion process in the absence of GA. It can be seen from the image that the metal surface is severely corroded due to the selective dissolution of the ferritic phase caused by the presence of carbonic acid in the solution. After the preferential dissolution of the ferritic phase, the presence of lamellar zones, corresponding to the non-dissolved cementite contained in the pearlitic structure, can be seen in the image. In contrast, the surface of the carbon steel sample was greatly improved after the addition of the inhibitor, showing a much smoother surface (Fig. 9c). This, as described earlier, is due to the formation of a protective adsorptive inhibitor layer on the metal surface that shields the metal sample from the aggressive solution.

The protective film formed on the carbon steel surface was analyzed using an energy-dispersive spectroscopy analysis technique (EDS). The EDS spectrum and the chemical composition of all three samples are shown in Figure S1 and Table S5 (supplementary information), respectively. It follows from the data that, in the blank solution, the surface of the sample is covered by a corrosion product layer mainly composed of carbon (6.55 wt.%) and iron (91.57 wt.%) and other alloying elements of the steel with only 1.03 wt.% of oxygen. These results seem to confirm the presence of Fe₃C on the sample surface with no iron carbonate layer formed on it. These findings are very well in agreement with the previous results. The literature reports (Ref 48–54) that in the presence of CO₂, at a temperature below $40\text{ }^{\circ}\text{C}$, the surface is mainly covered by a porous layer of Fe₃C and some alloying elements of the steel with little traces of FeCO₃. These previous works pointed out that, at this temperature, FeCO₃ precipitates only at elevated pH and/or at a high concentration of Fe²⁺ ions.

The EDS analysis reveals that in the presence of GA, the sample surface is covered by a layer with a higher concentration of carbon (14.89 wt.%) and oxygen (7.30 wt.%) elements. It should be noted that carbon and oxygen are also part of the chemical composition of the inhibitor; thus, the higher concentration of these two elements in this protective layer is likely ascribed to the adsorption of GA on the metal surface. Moreover, from the data, it is also evident that the percentage of iron decreases in the presence of GA (i.e., 91.31% for the uninhibited solution and 75.28% in the presence of GA). This decrease is likely to occur due to the overlying inhibitor film.

Over time, the selective dissolution of the ferrite phase on the surface sample leads to an increase in the concentration of Fe²⁺ ions in the tested solution. In this condition, the precipitation of FeCO₃ on the metal surface will be more favorable (Ref 48–54). Figure 10(a) and (b) shows the top-view SEM analysis of the metal surface after 168 h of immersion, in the absence and presence of GA, respectively. The figures show that both surfaces are totally covered with a porous layer. The EDS measurements reveal that both layers are rich in carbon, oxygen and iron elements, suggesting that the layers are mainly composed of Fe₃C with some traces of FeCO₃ (Ref 48). However, as in the previous case, the EDS analysis also shows that the concentration of the above-mentioned elements is higher when the metal is exposed to the inhibited solution (i.e., C:12.3%, O:6.6% and C:22.2%, O:11.0%, in the blank and the inhibited solution respectively). Furthermore, as can be seen from the cross section view of the samples, after the addition of

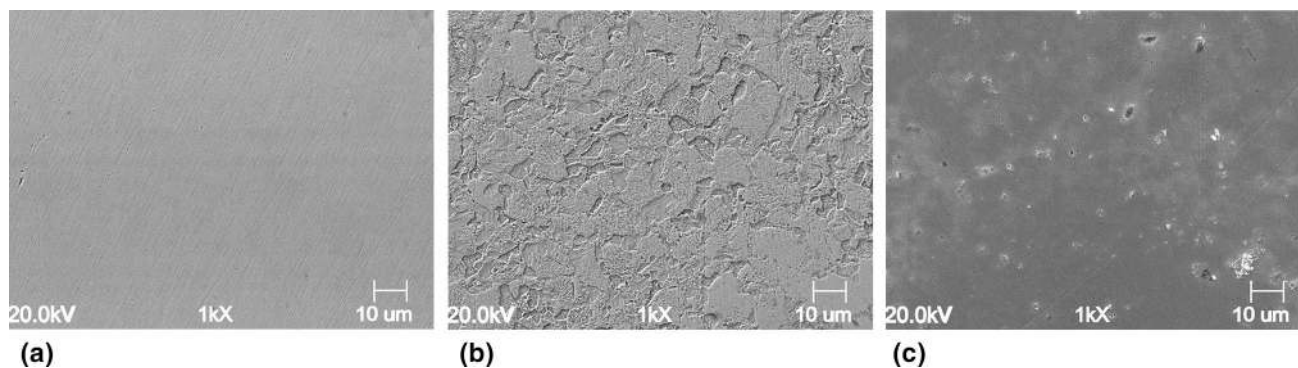


Fig. 9 SEM images of the carbon steel surface after 24 h of immersion time: (a) polished surface; (b) blank solution; (c) 0.5 g L^{-1} of GA

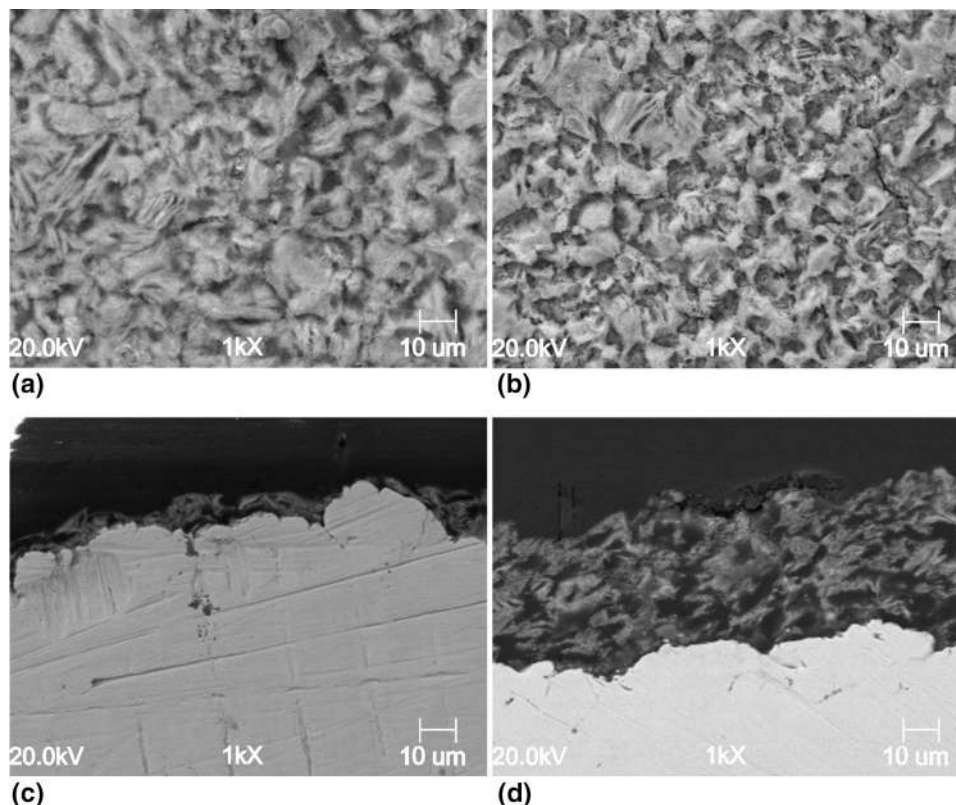


Fig. 10 Top view and cross section images of the carbon steel surface after 168 h of immersion time: (a) and (c) for the blank solution; (b) and (d) for 0.5 g L^{-1} of GA

GA, a thicker layer of approximately $50 \mu\text{m}$ (Fig. 10d) is formed on the metal surface against that one observed in the blank solution of approximately $10 \mu\text{m}$ (Fig. 10c). Other authors also reported a similar result (Ref 62, 63). These results clearly corroborate the electrochemical and gravimetric results presented in this study. The SEM and EDS analysis indicate that GA is gradually adsorbed on the metal surface, thus leading to the formation of a thicker and stable protective layer that hinders the diffusion of the aggressive species to the metal surface.

3.8 Mechanism of Inhibition

Gum arabic (GA) is a water-soluble and a complex mixture of arabinogalactan (AG), arabinogalactan-protein (AGP) and

glycoprotein (GP) fraction comprising of 88.4, 10.4, 1.2% of the total volume, respectively, with 0, 50, 25%, of the protein content, respectively (Ref 64) (Figure S3 in supplementary information). It is well known that the mode of adsorption, either physical and/or chemical, of a given inhibitor depends on the presence of certain physicochemical properties on the inhibitor molecule such as functional groups, charge density, size and the way its molecules interact with the metal. Due to its complex chemical structure, it is not possible to determine the exact mechanism involved, since some components may be physically and others chemically adsorbed. Inspection of Table 2 reveals that the calculated values of ΔG_{ads} indicate that the adsorption mechanism of GA on the metal surface occurs through a mixed-type interaction (i.e., physical and

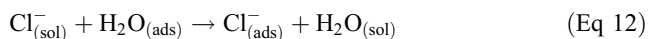
chemical adsorption), with the physical adsorption being more dominant. Moreover, based on the analysis of the FT-IR spectra performed on the native and adsorbed inhibitor and from the electrochemical findings, it is possible to speculate that the following four types of adsorption mechanisms or a combination of them may take place in the inhibiting phenomena involving GA on the steel surface.

3.8.1 Electrostatic Metal–Inhibitor Interaction. The polysaccharide fraction of GA (i.e., AG) contains hydroxyl functional groups (–OH), and carboxyl functional groups (–COOH). The protein fraction (i.e., AGP and GP) contains amino acids thus rich in amino (–NH₂) and carboxyl groups. In an acid solution, these functional groups are protonated such that the polymer is in equilibrium with its polycation (Ref 25, 28):



where $(\text{GAH}_x)_{(\text{sol})}^{x+}$ is the protonated inhibitor in the solution.

Moreover, in an acid solution, chloride ions have a strong tendency to be adsorbed on the positively charged metallic surface (Ref 25, 28, 65):



The adsorptions of these anions create an excess of electrons such that the metal surface carries negative charges. The formation of these negative charges facilitates the adsorption of the inhibitor on the metal surface through electrostatic interaction between the protonated GA molecule and the mild steel surface (Ref 25, 43) (Figure S4a from supplementary information).

3.8.2 Adsorption via H-Bond Formation. In addition to the electrostatic adsorption, the electrochemical and morphological findings also suggest that GA might be adsorbed on the metal surface via the formation of H bonds. As can be seen from Fig. 5, the cathodic current density decreases after the addition of the inhibitor. Roy et al. (Ref 17) and Messali et al. (Ref 18) studied the corrosion inhibition effect of guar gum in acid solution and also reported a similar result. They suggested that the decrease in the cathodic current density might be due to the formation of H bonds between the hydroxyl groups of the mannose units and the H⁺ ions present on the cathodic sites of the metal surface. This leads to the suppression of the hydrogen evolution reaction (Figure S4b in supplementary information). The FT-IR measurements reported in this study seem to support such a hypothesis. Figure 8 shows that the intensity of the characteristic peak associated with the hydroxyl groups decreases after the adsorption of GA on the metal surface. This behavior may be likely due to the formation of hydrogen bonds established between the hydroxyl groups of the carbohydrate molecules and the metal surface up to a different extent. Moreover, it is also possible that some of the free hydroxyl and carboxylic groups can also interact with the oxide layer formed on the metal surface through the formation of hydrogen bonds. The literature reports that oxide and/or hydroxide species formed on the metal surface might promote the adsorption of the inhibitor via the formation of such bonds (Ref 45, 66). Leong et al. (Ref 62) and Williams et al. (Ref 63) studied the adsorption effect of GA macromolecules toward oxide nanoparticles surface (i.e., magnetite nanoparticles). The authors reported that GA showed a strong affinity toward such nanoparticles. They observed that the charged and/or uncharged

carboxylate/hydroxyl groups of the inhibitor molecules were able to interact with the oxide nanoparticles surface, leading to the formation of a thick adsorptive layer on their surface. In the presence of CO₂, FeCO₃, oxide and/or hydroxide species would form on the surface (Ref 5, 53, 54). Therefore, the adsorption of GA can also be promoted via the formation of hydrogen bonds between the hydroxyl and carboxylic groups of the inhibitor and the oxidized intermediate species on the metal surface.

3.8.3 Chelating Action. Polysaccharides, due to lone pair electrons among their macromolecules, might act also as a ligand, forming stable metal ion–polysaccharide complexes (Ref 67, 68). The FT-IR analysis presented in Fig. 8 reveals that the peaks associated with the glucoside (1-4) linkage of the galactose unit and the (1-6) linkage of the mannose unit decrease after the adsorption of GA on the metal. It has been postulated that (Ref 17-19) the endocyclic “O” atom of GA molecules could interact with freshly generated Fe²⁺ ions present on the anodic sites to form stable metal ion–inhibitor complexes. These complexes can be adsorbed on the steel surface through van der Waals forces forming of a protective layer, preventing the aggressive species present in the solution to reach the metal surface (Figure S4d in supplementary information). Roy et al. (Ref 17) and Messali et al. (Ref 18) also reported a similar result.

3.8.4 Chemical Adsorption. As mentioned before, a small contribution of the chemical adsorption process is also observed. In a weak acid solution, GA can exist as neutral macromolecules in equilibrium with its polycations (Eq 11). These neutral macromolecules can be adsorbed on the metal surface via the formation of coordinate bonds with the metal surface. In this case, the inhibitor will act as a Lewis base by donating the unshared electrons of the heteroatoms (e.g., oxygen and nitrogen) to vacant *d*-orbitals of iron atom on steel surface (e.g., Lewis acid) (Figure S4c in supplementary information) (Ref 17-19). However, it should be noted that this mechanism is more likely to occur in the first hours of the experiment. In fact, as the immersion time increases, the metal surface is progressively covered by a corrosion product layer; therefore, the direct coordination of oxygen to an exposed metal atom decreases.

4. Conclusion

Considering the obtained results, the effect of gum arabic on the corrosion behavior of carbon steel in a CO₂-saturated chloride (0.5 M of KCl) solution can be summarized in the following points:

- The thickening agent gum arabic was found to be an efficient corrosion inhibitor for carbon steel in the tested solution.
- The inhibition efficiency increases with an increase in inhibitor concentration up to 0.5 g L⁻¹, but it decreases with increasing the temperature.
- The inhibition efficiency also increases over prolonged exposure times up to 92.44% after 168 h.
- The adsorption of GA on the carbon steel surface follows the Temkin’s adsorption isotherm model.
- The negative free energy of adsorption $\Delta G_{\text{ads}}^{\circ}$ indicates a strong and spontaneous adsorption of GA on the carbon steel surface. Moreover, the values of $\Delta G_{\text{ads}}^{\circ}$ indicate that

the tested inhibitor adsorbs mainly via physical adsorption with a little contribution of chemical adsorption.

- The values of the activation energy and heat of adsorption in the presence of GA were found to be higher than those obtained in the free inhibitor solution, further supporting the physical adsorption nature of the process.
- Polarization measurements indicate that GA acts as a mixed-type inhibitor with a higher influence on the anodic reaction.
- The FT-IR measurements reveal that GA was strongly adsorbed on the metal surface.
- The cross section analysis confirmed the formation of a thick protective layer of approximately 50 μm after the addition of 0.5 g L^{-1} of GA, while in the blank solution it was approximately 10 μm .

Acknowledgments

The work was supported by the National Centre for Research and Development (Project No. PBS1/A2/11/2012).

Open Access

This article is distributed under the terms of the Creative Commons Attribution 4.0 International License (<http://creativecommons.org/licenses/by/4.0/>), which permits unrestricted use, distribution, and reproduction in any medium, provided you give appropriate credit to the original author(s) and the source, provide a link to the Creative Commons license, and indicate if changes were made.

References

1. Report of U.S. Department of Energy Office of Fossil Energy and National Energy Technology, *Modern Shale Gas*, 2009
2. F.R. Spellman, *Environmental Impacts of Hydraulic Fracturing*, CRC Press, Boca Raton, 2013
3. A.P. Bungler, J. McLennan, and R. Jeffrey, *Effective and Sustainable Hydraulic Fracturing*, InTech, Rijeka, 2013
4. G. Palumbo and J. Banaś, Study on Inhibition of N80 Carbon Steel in 0.5 M KCl Solution Saturated with CO₂ by Gum Arabic, *J. Cast Mater. Eng.*, 2018, **2**, p 5–8
5. G. Palumbo, J. Banaś, A. Bałkowiec, J. Mizera, and U. Lelek-Borkowska, Electrochemical Study of the Corrosion Behaviour of Carbon Steel in Fracturing Fluid, *J. Solid State Electrochem.*, 2014, **18**(11), p 2933–2945
6. G. Palumbo, M. Andrzejczuk, J. Mizera, and J. Banaś, Corrosion Inhibition of Carbon Steel (K-55) in CO₂-Saturated 0.5 M KCl Solution by Polyacrylamide, *Ochrona przed Korozją*, 2015, **11**, p 396–399
7. G. Palumbo, A. Bałkowiec, U. Lelek-Borkowska, J. Banaś, and J. Mizera, Corrosion Inhibition of K-55 Carbon Steel in Diluted Potassium Chloride Solution by Polyacrylamide, *Ochrona przed Korozją*, 2015, **10**, p 358–361
8. G. Palumbo and J. Banaś, Inhibition Effect of Guar Gum on the Corrosion Behaviour of Carbon Steel (K-55) in Fracturing Fluid, *Solid State Phenom.*, 2015, **227**, p 59–62
9. B.R. Linter and G.T. Burstein, Reactions of Pipeline Steels in Carbon Dioxide Solutions, *Corros. Sci.*, 1999, **41**(1), p 117–139
10. V.M. Abbasov, H.M. Abd El-Lateef, L.I. Aliyeva, E.E. Qasimov, I.T. Ismayilov, and M.M. Khalaf, A Study of the Corrosion Inhibition of Mild Steel C1018 in CO₂-Saturated Brine Using Some Novel Surfactants Based on Corn Oil, *Egypt J. Pet.*, 2013, **22**(4), p 451–470
11. J.M. Sufliita, T.J. Phelps, and B. Little, Carbon Dioxide Corrosion and Acetate: A Hypothesis on the Influence of Microorganisms, *Corrosion*, 2008, **64**(11), p 854–859
12. D.M. Ortega-Toledo, J.G. Gonzalez-Rodriguez, M. Casales, L. Martinez, and A. Martinez-Villafañe, Co₂ Corrosion Inhibition of X-120 Pipeline Steel by a Modified Imidazoline Under Flow Conditions, *Corros. Sci.*, 2011, **53**(11), p 3780–3787
13. M. Heydari and M. Javidi, Corrosion Inhibition and Adsorption Behaviour of an Amido-Imidazoline Derivative on API, 5L X52 Steel in CO₂-Saturated Solution and Synergistic Effect of Iodide Ions, *Corros. Sci.*, 2012, **61**, p 148–155
14. X. Liu, P.C. Okafor, and Y.G. Zheng, The Inhibition of CO₂ Corrosion of N80 Mild Steel in Single Liquid Phase and Liquid/Particle Two-Phase Flow by Aminoethyl Imidazoline Derivatives, *Corros. Sci.*, 2009, **51**(4), p 744–751
15. H.-H. Zhang, X. Pang, M. Zhou, C. Liu, L. Wei, and K. Gao, The Behavior of Pre-Corrosion Effect on the Performance of Imidazoline-Based Inhibitor in 3wt.% NaCl Solution Saturated with CO₂, *Appl. Surf. Sci.*, 2015, **356**, p 63–72
16. A. Singh, K.R. Ansari, A. Kumar, W. Liu, C. Songsong, and Y. Lin, Electrochemical, Surface and Quantum Chemical Studies of Novel Imidazole Derivatives as Corrosion Inhibitors for J55 Steel in Sweet Corrosive Environment, *J. Alloys Compd.*, 2017, **712**, p 121–133
17. P. Roy, P. Karfa, U. Adhikari, and D. Sukul, Corrosion Inhibition of Mild Steel in Acidic Medium by Polyacrylamide Grafted Guar Gum with Various Grafting Percentage: Effect of intramolecular Synergism, *Corros. Sci.*, 2014, **88**, p 246–253
18. M. Messali, H. Lgaz, R. Dassanayake, R. Salghi, S. Jodeh, N. Abidi, and O. Hamed, Guar Gum as Efficient Non-Toxic Inhibitor of Carbon Steel Corrosion in Phosphoric Acid Medium: Electrochemical, Surface, DFT and MD Simulations Studies, *J. Mol. Struct.*, 2017, **1145**, p 43–54
19. M. Abdallah, Guar Gum as Corrosion Inhibitor for Carbon Steel in Sulfuric Acid Solutions, *Port. Electrochim. Acta*, 2004, **22**, p 161–175
20. G. Palumbo, K. Berent, E. Proniewicz, and J. Banaś, Guar Gum as an Eco-Friendly Corrosion Inhibitor for Pure Aluminium in 1-M HCl Solution, *Materials*, 2019, **12**(16), p 2026
21. S.A. Umoren, I.B. Obot, and N.O. Obi-Egbedi, Raphia Hookeri Gum as a Potential Eco-Friendly Inhibitor for Mild Steel in Sulfuric Acid, *J. Mater. Sci.*, 2009, **44**(1), p 274–279
22. M. Mobin and M. Rizvi, Inhibitory Effect of Xanthan Gum and Synergistic Surfactant Additives for Mild Steel Corrosion in 1 M HCl, *Carbohydr. Polym.*, 2016, **136**, p 384–393
23. M. Mobin and M. Rizvi, Polysaccharide from Plantago as a Green Corrosion Inhibitor for Carbon Steel in 1 M HCl Solution, *Carbohydr. Polym.*, 2017, **160**, p 172–183
24. E. Bayol, A.A. Gürten, M. Dursun, and K. Kayakirilmaz, Adsorption Behavior and Inhibition Corrosion Effect of Sodium Carboxymethyl Cellulose on Mild Steel in Acidic Medium, *Acta Phys-Chim. Sin.*, 2008, **24**(12), p 2236–2243
25. H. Bentrach, Y. Rahali, and A. Chala, Gum Arabic as an Eco-Friendly Inhibitor for API, 5L X42 Pipeline Steel in HCl Medium, *Corros. Sci.*, 2014, **82**, p 426–431
26. S.A. Umoren, Inhibition of Aluminium and Mild Steel Corrosion in Acidic Medium Using Gum Arabic, *Cellulose*, 2008, **15**(5), p 751–761
27. S.A. Umoren, I.B. Obot, E.E. Ebenso, P.C. Okafor, O. Ogbobe, and E.E. Oguzie, Gum Arabic as a Potential Corrosion Inhibitor for Aluminium in Alkaline Medium and Its Adsorption Characteristics, *Anti-Corros. Methods Mater.*, 2006, **53**(5), p 277–282
28. S.A. Umoren, O. Ogbobe, I.O. Igwe, and E.E. Ebenso, Inhibition of Mild Steel Corrosion in Acidic Medium Using Synthetic and Naturally Occurring Polymers and Synergistic Halide Additives, *Corros. Sci.*, 2008, **50**(7), p 1998–2006
29. M. Mobin and M.A. Khan, Investigation on the Adsorption and Corrosion Inhibition Behavior of Gum Acacia and Synergistic Surfactants Additives on Mild Steel in 0.1 M H₂SO₄, *J. Dispers. Sci. Technol.*, 2013, **34**(11), p 1496–1506
30. E.E. Oguzie, Y. Li, and F.H. Wang, Corrosion Inhibition and Adsorption Behavior of Methionine on Mild Steel in Sulfuric Acid and Synergistic Effect of Iodide Ion, *J. Colloid Interface Sci.*, 2007, **310**(1), p 90–98
31. M.A. Abu-Dalo, A.A. Othman, and N.A.F. Al-Rawashdeh, Exudate Gum from Acacia Trees as Green Corrosion Inhibitor for Mild Steel in Acidic Media, *Int. J. Electrochem. Sci.*, 2012, **7**, p 9303–9324

32. M.A. Amin, S.S.A. Ei-Rehim, E.E.F. El-Sherbini, O.A. Hazzazi, and M.N. Abbas, Polyacrylic Acid as a Corrosion Inhibitor for Aluminium in Weakly Alkaline Solutions. Part I: Weight Loss, Polarization, Impedance EFM and EDX Studies, *Corros. Sci.*, 2009, **51**(3), p 658–667
33. A. Singh, Y. Lin, E.E. Ebenso, W. Liu, J. Pan, and B. Huang, Gingko Biloba Fruit Extract as an Eco-Friendly Corrosion Inhibitor for J55 Steel in CO₂ Saturated 3.5% NaCl Solution, *J. Ind. Eng. Chem.*, 2015, **24**, p 219–228
34. A. Singh, Y. Lin, E.E. Ebenso, W. Liu, and B. Huang, Determination of Corrosion Inhibition Efficiency Using HPHT Autoclave by Gingko Biloba on Carbon Steels in 3.5% NaCl solution Saturated with CO₂, *Int. J. Electrochem. Sci.*, 2014, **9**, p 5993–6005
35. A. Singh, Y. Lin, W. Liu, E.E. Ebenso, and J. Pan, Extract of *Momordica charantia* (Karela) Seeds as Corrosion Inhibitor for P110SS Steel in CO₂ Saturated 3.5% NaCl Solution, *Int. J. Electrochem. Sci.*, 2013, **8**, p 12884–12893
36. S.A. Umoren, A.A. AlAhmary, Z.M. Gasem, and M.M. Solomon, Evaluation of Chitosan and Carboxymethyl Cellulose as Ecofriendly Corrosion Inhibitors for Steel, *Int. J. Biol. Macromol.*, 2018, **117**, p 1017–1028
37. D. Verbeken, S. Dierckx, and K. Dewettinck, Exudate Gums: Occurrence, Production, and Applications, *Appl. Microbiol. Biotechnol.*, 2003, **63**(1), p 10–21
38. E. Dauqan and A. Abdullah, Utilization of Gum Arabic for Industries and Human Health, *Am. J. Appl. Sci.*, 2013, **10**, p 1270–1279
39. Standard Practice for Preparing, Cleaning, and Evaluation Corrosion Test Specimens, ASTM, 1999
40. S. Muralidharan, B. Ramesh Babu, S. Venkatakrishna Iyer, and S. Rengamani, Influence of Anions on the Performance of Isomers of Aminobenzoic Acid on the Corrosion Inhibition and Hydrogen Permeation Through Mild Steel in Acidic Solutions, *J. Appl. Electrochem.*, 1996, **26**(3), p 291–296
41. F. Bentiss, M. Traisnel, and M. Lagrenee, The Substituted 1,3,4-Oxadiazoles: A New Class of Corrosion Inhibitors of Mild Steel in Acidic Media, *Corros. Sci.*, 2000, **42**(1), p 127–146
42. A. Peter, S.K. Sharma, and I.B. Obot, Anticorrosive Efficacy and Adsorptive Study of Guar Gum with Mild Steel in Acidic Medium, *J. Anal. Sci. Technol.*, 2016, **7**(1), p 26
43. E.E. Oguzie, Y. Li, and F.H. Wang, Effect of 2-Amino-3-Mercapto-propanoic Acid (Cysteine) on the Corrosion Behaviour of Low Carbon Steel in Sulphuric Acid, *Electrochim. Acta*, 2007, **53**(2), p 909–914
44. E. McCafferty and N. Hackerman, Double Layer Capacitance of Iron and Corrosion Inhibition with Polymethylene Diamines, *Electrochem. Soc.*, 1972, **119**, p 146–154
45. M.A. Amin, K.F. Khaled, and S.A. Fadl-Allah, Testing Validity of the Tafel Extrapolation Method for Monitoring Corrosion of Cold Rolled Steel in HCl Solutions—Experimental and Theoretical Studies, *Corros. Sci.*, 2010, **52**(1), p 140–151
46. C. Cao, On Electrochemical Techniques for Interface Inhibitor Research, *Corros. Sci.*, 1996, **38**(12), p 2073–2082
47. X. Li, S. Deng, H. Fu, and T. Li, Adsorption and Inhibition Effect of 6-Benzylaminopurine on Cold Rolled Steel in 1.0 M HCl, *Electrochim. Acta*, 2009, **54**(16), p 4089–4098
48. J.L. Mora-Mendoza and S. Turgoose, Fe₃C Influence on the Corrosion Rate of Mild Steel in Aqueous CO₂ Systems Under Turbulent Flow Conditions, *Corros. Sci.*, 2002, **44**(6), p 1223–1246
49. H. Wang, H. Shi, W.P. Jepsen, T. Hong, and C. Kang, Characterization of Inhibitor and Corrosion Product Film Using Electrochemical Impedance Spectroscopy (EIS), in *CORROSION 2001*. 2001, NACE International: Houston, Texas. p 22
50. F. Farelas, B. Brown, and S. Nestic, Iron Carbide and Its Influence on the Formation of Protective Iron Carbonate in CO₂ Corrosion of Mild Steel, in *CORROSION 2013*. NACE International, Orlando, 2013, p 15
51. A.B. Forero, M.M.G. Núñez, and I.S. Bott, Analysis of the Corrosion Scales Formed on API, 5L X70 and X80 Steel Pipe in the Presence of CO₂, *Mater. Res.*, 2014, **17**(2), p 461–471
52. T. Tanupabrunsun, B. Brown, and S. Nestic, Effect of pH on CO₂ Corrosion of Mild Steel at Elevated Temperatures, in *CORROSION 2013*. 2013, NACE International, Orlando, p 11
53. J. Banas, U. Lelek-Borkowska, B. Mazurkiewicz, and W. Solarski, Effect of CO₂ and H₂S on the Composition and Stability of Passive film on Iron Alloys in Geothermal Water, *Electrochim. Acta*, 2007, **52**, p 5704–5714
54. J.K. Heuer and J.F. Stubbins, An XPS Characterization of FeCO₃ Films from CO₂ Corrosion, *Corros. Sci.*, 1999, **41**(7), p 1231–1243
55. I.B. Onyeachu, D.S. Chauhan, K.R. Ansari, I.B. Obot, M.A. Quraishi, and A.H. Alamri, Hexamethylene-1,6-bis(N-d-Glucopyranosylamine) as a Novel Corrosion Inhibitor for Oil and Gas Industry: Electrochemical and Computational Analysis, *New J. Chem.*, 2019, **43**(19), p 7282–7293
56. M.N. El-Haddad and A.S. Fouda, Inhibition Effect and Adsorption Behavior of New Azodye Derivatives on Corrosion of Carbon Steel in Acid Medium, *J. Dispers. Sci. Technol.*, 2013, **34**(10), p 1471–1480
57. H. Espinosa-Andrews, O. Sandoval-Castilla, H. Vázquez-Torres, E.J. Vernon-Carter, and C. Lobato-Calleros, Determination of the Gum Arabic–Chitosan Interactions by Fourier Transform Infrared Spectroscopy and Characterization of the Microstructure and Rheological Features of Their Coacervates, *Carbohydr. Polym.*, 2010, **79**(3), p 541–546
58. M. Bashir and S. Haripriya, Assessment of Physical and Structural Characteristics of Almond Gum, *Int. J. Biol. Macromol.*, 2016, **93**, p 476–482
59. D. Mudgil, S. Barak, and B.S. Khatkar, X-Ray Diffraction, IR Spectroscopy and Thermal Characterization of Partially Hydrolyzed Guar Gum, *Int. J. Biol. Macromol.*, 2012, **50**(4), p 1035–1039
60. F.E. Vasile, M.J. Martinez, V.M. Pizones Ruiz-Henestrosa, M.A. Judis, and M.F. Mazzobre, Physicochemical, Interfacial and Emulsifying Properties of a Non-Conventional Exudate Gum (*Prosopis alba*) in Comparison with Gum Arabic, *Food Hydrocoll.*, 2016, **56**, p 245–253
61. S.S. Banerjee and D.-H. Chen, Fast Removal of Copper Ions by Gum Arabic Modified Magnetic Nano-Adsorbent, *J. Hazard. Mater.*, 2007, **147**, p 792–799
62. Y.K. Leong, U. Seah, S.Y. Chu, and B.C. Ong, Effects of Gum Arabic Macromolecules on Surface Forces in Oxide Dispersions, *Colloids Surf. A.*, 2001, **182**(1), p 263–268
63. D.N. Williams, K.A. Gold, T.R.P. Holoman, S.H. Ehrman, and O.C. Wilson, Surface Modification of Magnetic Nanoparticles Using Gum Arabic, *J. Nanopart. Res.*, 2006, **8**(5), p 749–753
64. F. Niu, Y. Zhang, C. Chang, W. Pan, W. Sun, Y. Su, and Y. Yang, Influence of the Preparation Method on the Structure Formed by Ovalbumin/Gum Arabic to Observe the Stability of Oil-in-Water Emulsion, *Food Hydrocoll.*, 2017, **63**, p 602–610
65. K.F. Khaled, The Inhibition of Benzimidazole Derivatives on Corrosion of Iron in 1 M HCl Solutions, *Electrochim. Acta*, 2003, **48**(17), p 2493–2503
66. R.D. Braun, E.E. Lopez, and D.P. Vollmer, Low Molecular Weight Straight-Chain Amines as Corrosion Inhibitors, *Corros. Sci.*, 1993, **34**(8), p 1251–1257
67. J.A. Rendleman, Metal-Polysaccharide Complexes—Part I, *Food Chem.*, 1978, **3**(1), p 47–79
68. J.A. Rendleman, Metal-Polysaccharide Complexes—Part II, *Food Chem.*, 1978, **3**(2), p 127–162

Publisher's Note Springer Nature remains neutral with regard to jurisdictional claims in published maps and institutional affiliations.